Single-mode and tunable VCSELs in the near- to mid-infrared

Invited Paper

Markus-Christian Amann and Werner Hofmann

Walter Schottky Institut, Technische Universität München, D-85748 Garching, Germany

Received June 10, 2008

Single-mode, long-wavelength vertical-cavity surface-emitting lasers (VCSELs) in the near- to mid-infrared covering the wavelength range from 1.3 to 2.3 μm are presented. This wide spectral emission range opens applications in gas sensing and optical interconnects. All these lasers are monolithically grown in the InGaAlAs-InP material system utilizing a buried tunnel junction (BTJ) as current aperture. Fabricated with a novel high-speed design with reduced parasitics, bandwidths in excess of 10 GHz at 1.3 and 1.55 μm have been achieved. Therefore, the coarse wavelength division multiplexing (CWDM) wavelength range of 1.3 to 1.6 μm at 10 Gb/s can be accomplished with one technology. Error-free data-transmission at 10 Gb/s over a fiber link of 20 km is demonstrated. One-dimensional arrays have been fabricated with emission wavelengths addressable by current tuning. Micro-electro-mechanical system (MEMS) tunable devices provide an extended tuning range in excess of 50 nm with high spectral purity. All these devices feature continuous-wave (CW) operation with typical single-mode output powers exceeding 1 mW. The operation voltage is around $1-1.5$ V and power consumption is as low as $10-20$ mW. Furthermore, we have also developed VCSELs based on GaSb, targeting at the wavelength range from 2.3 to 3.0 μm. The functionality of tunable diode laser spectroscopy (TDLS) systems is shown by presenting a laser hygrometer applying a 1.84-μm VCSEL.

OCIS codes: 140.7260, 140.3570, 140.3600, 140.3070, 060.2380, 280.4788.
doi: 10.3788/COL20080610.0743.

Since the vertical-cavity surface-emitting laser (VCSEL) was invented by Prof. Iga in 1977[1], international research on these devices entailed numerous achievements. Nowadays, these devices have reached a degree of maturity allowing to enter industrial applications[2]. On the one hand, the VCSEL-chip has a low-cost potential due to the compact design, high-volume producibility, on-wafer testability, and lower packaging cost[3]. On the other hand, with its low power consumption, outperforming edge-emitters in $1-2$ orders of magnitude, small-form factors with restrictions in power consumption can only be accommodated by VCSEL technology. Especially, long-wavelength VCSELs have shown a tremendous development during the last years and are commercially available today. Covering the wavelength range from 1.3 to 2.3 μm and providing high continuous-wave (CW) output powers up to 100 °C qualify them for various applications[4–8]. Also, modulation bandwidths in excess of 10 GHz have been demonstrated[9]. While the mature GaAs-based technology extends to about 1.3 μm exploiting GaInNAs active regions[10], various approaches have shown that superior performance can be obtained with InP-based device concepts that benefit from the excellent gain properties of strained AlGaInAs/InP quantum wells. In order to avoid the thermal problem caused by thermally low conducting ternary and quaternary alloys in the epitaxial mirrors, dielectric mirrors, heat spreaders, or wafer bonding techniques have been introduced[11,12].

One of the most powerful approaches for long-wavelength InP-based devices is the buried tunnel junction (BTJ) concept with self accomplished current and index guiding.

Trace-gas sensing and measurement are important growth-markets with various applications. Especially, tunable diode laser spectroscopy (TDLS) is a cost-effective and powerful technology. With their excellent single-mode behavior providing side-mode suppression ratios (SMSRs) in excess of 30 dB and their inherent electro-thermal tunability, BTJ-VCSELs are particularly qualified as light sources for optical gas sensing applications. Being available in the near- to mid-infrared spectrum over a wavelength range from 1.3 to 2.3 μm, many absorption lines of molecules such as water, methane, carbon-dioxide, carbon-monoxide, and numerous other trace-gases can be covered[13–15].

In this letter, we present the latest results on long-wavelength single-mode and tunable BTJ-VCSELs in the near- to mid-infrared and demonstrate their applications.

The structure of the present BTJ-VCSELs on InP is basically the same as that described in Ref. [3]. Mid-infrared devices based on GaSb, however, require a novel laser layout[16]. The appliance of the BTJ with its self-adjusted current and optical confinement yields several benefits. Firstly, the major part of the high-resistive p-side confinement layers can be replaced by n-conducting materials. Secondly, the upside-down mounted structure (the InP substrate on top is completely removed) with its electroplated Au pseudo-substrate also serving as heat sink, results in low threshold and high operation temperature. The hybrid back mirror of these lasers is typically made of 3.5 pairs of CaF_2/ZnS and a gold layer. The epitaxial output mirror consists of InGaAlAs/InAlAs layer pairs with tailored composition to avoid fundamental absorption for the designed wavelength. The number of pairs is chosen to achieve an optimized output mirror reflectivity (typically around 99%). To realize high temperature operation, the mode-gain offset is designed to

 © 2008 Chinese Optics Letters

achieve minimal threshold current variation over temperature. The active region typically consists of 5 to 7 compressively strained quantum wells separated by tensile strained barriers. For very long wavelengths, highly strained quantum wells have to be realized demanding very high requirements on the epitaxial growth. The critical growth thickness of 5 quantum wells is already reached at an emission wavelength of slightly above 2 μm. For further increase of the emission wavelength, an optimization of the shape of the quantum well is required. For the InP-based 2.3 μm VCSELs, we introduced V-shaped quantum wells to prevent an abrupt change from heavily tensile strained barriers and heavily compressive strained quantum wells[14]. Although these lasers still perform well, this seems to be the upper wavelength limit for lasers on InP substrate. Therefore, we recently introduced GaSb-based VCSELs addressing the entire wavelength range from 2 to 3 μm[16].

To achieve high-speed operation, the chip layout has to be taken into account. Figure 1 presents the schematic layout of our high-speed VCSEL as described in Ref. [9]. Benzo-cyclo-butene (BCB, Cyclotene^{TM}, silicate plastics) is used as low-dielectric constant ($\varepsilon \approx 2.5$ versus 12 of InP) passivation to enable high-speed operation. This design is essential for broadband optical interconnects with VCSELs at 1.3 or 1.55 μm.

All VCSELs are electro-thermally tunable over a few nanometers due to temperature dependence of the refractive index in the cavity heated up by driving current. For

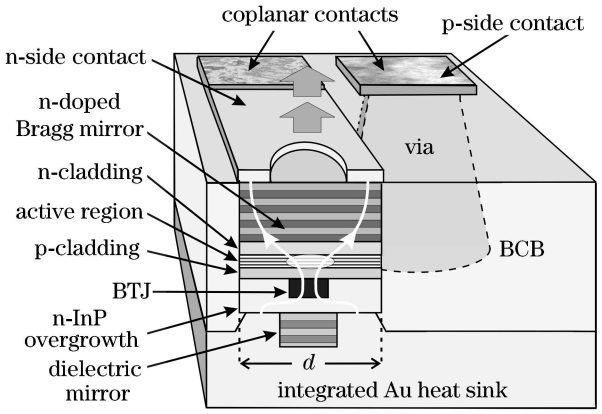

Fig. 1. Schematic cross-sectional structure of a long-wavelength VCSEL in high-speed design.

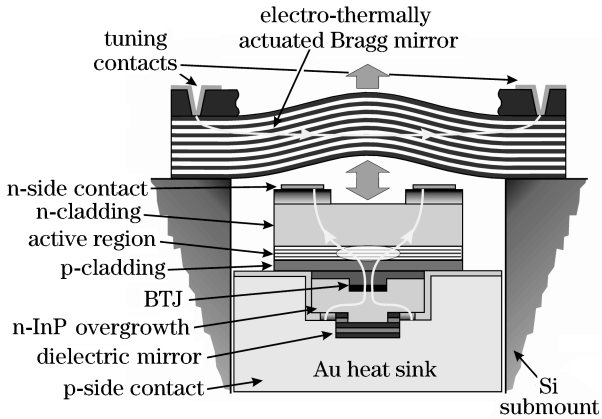

Fig. 2. Schematic cross section of a widely tunable two-chip VCSEL.

widely tunable devices, we presented a two-chip concept as depicted in Fig. 2[17]. For this device, the monolithic top distributed Bragg reflector (DBR) is replaced by an air gap and a micro-mechanical mirror membrane consisting of 22.5 pairs of GaAs and AlGaAs. The air gap thickness can be varied by a tuning current through the membrane causing thermal expansion by Joule heating and subsequent vertical movement. This design concept allows widely tunable VCSEL devices.

Broadband modulation performance is particularly required for applications in telecommunications. The required wavelength span for long-range links is the coarse wavelength division multiplexing (CWDM) range from 1.3 to 1.6 μm. Furthermore, single-mode emission and sufficient output power are mandatory. Figure 3 shows light output versus current and current versus voltage (L-I-V) characteristics and spectral performance of a typical high-speed VCSEL. The polarization mode is suppressed by more than 40 dB. Since the modulation bandwidth is very high, a small-signal modulation (−15 dBm) at 20 GHz causes well visible modulation sidebands in the spectrum and even second-order harmonics at 40 GHz can be recognized.

The threshold current is typically below 1 mA and the single-mode output power exceeds several milliwatts. Depending on the current aperture and bias, the differential series resistance $R_{\rm dif}$ is between 25 and 75 Ω. Therefore, no matching circuit is usually needed to drive the VCSEL with a standard 50-Ω driver board.

The small-signal modulation performance of a typical high speed VCSEL is presented in Fig. 4. A 3-dB

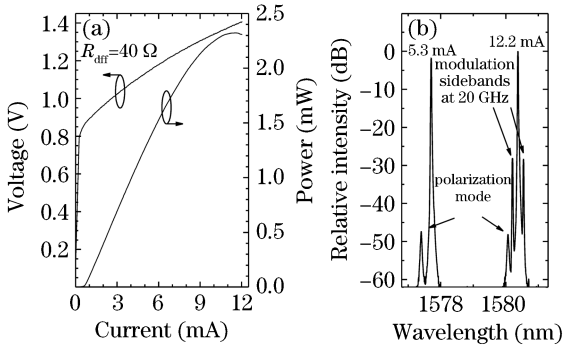

Fig. 3. (a) L-I-V characteristics and (b) spectrum of a 1.55-μm high-speed VCSEL at room temperature (20 °C).

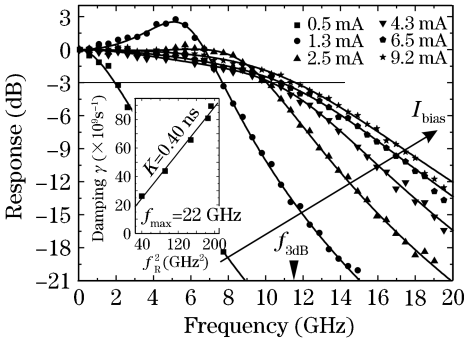

Fig. 4. Small-signal frequency response of a 1.55-μm VCSEL for various bias currents. The symbols represent the measured values and solid lines are curve-fits allowing damping rate γ and resonance frequency $f_{\rm R}$ to be extracted (plotted as inset with derived K-factor).

bandwidth of 11.6 GHz is demonstrated which is sufficient for data-rates in excess of 12.5 Gb/s. The measurement was done using an HP 8720D vector network analyzer (VNA) and a calibrated HP 11982A photodetector[18]. The response of the detector was subtracted from the presented data. The chip with its coplanar connectivity was directly connected by a cascade microprobe.

Curve fitting allows several intrinsic parameters such as modulation current efficiency factor and thermally limited maximum relaxation oscillation frequency to be extracted. The solid line in Fig. 4 is a fit to a three-pole filter function including damped relaxation-oscillation pole, and parasitics characterized by $f_{\rm par}$. The filter function is given as

$$H(f) \propto \frac{f_{\rm R}^2}{f_{\rm R}^2 - f^2 + j\frac{f}{2\pi}\gamma} \cdot \frac{1}{1 + j\frac{f}{f_{\rm par}}}. \quad (1)$$

The first part of Eq. (1) can be directly derived by small-signal analysis of the rate-equations above threshold, yielding a two-parameter modulation transfer function characterized by the relaxation oscillation frequency $f_{\rm R}$ and the damping-factor γ. The damping factor

$$\gamma = K \cdot f_{\rm R}^2 + \gamma_0 \quad (2)$$

is proportional to the resonance-frequency squared with an offset γ_0 and the constant of proportionality K, which is derived in the inset of Fig. 4. A maximum intrinsic bandwidth

$$f_{\max} = \sqrt{2}\frac{2\pi}{K} \quad (3)$$

due to over-damping can be calculated from K. The second part of Eq. (1) models the electrical chip-parasitics by a single parasitic pole. The advantage of this procedure, compared to other techniques like the subtraction method[19], is that parasitics are allowed to vary over bias in this model. For VCSELs, parasitics change especially at small bias currents due to current crowding. It is assumed that the parasitic response can be modeled by a low pass of first order. In order to refine and verify that model, we extracted parasitic responses from S_{11}-measurements and did equivalent circuit fitting as presented in Fig. 5. The first order equivalent circuit is presented as inset. The VCSELs under investigation had an identical optical resonator, but various chip diameters d as shown in Fig. 1. Biasing conditions were kept identical. No fluctuation of the intrinsic parameters was observed, whereas the modulation performance $f_{3\ \rm dB}$ went down 50% with increased chip diameter, as shown in the second inset. Although the equivalent circuit contains only three elements (resistors R_m and R_a, capacitance C_a), it can model the electrical impedance of our VCSEL well and the element values ($R_m = 12.4$ Ω, $R_a = 33$ Ω, $C_a = 0.76$ pF at $d = 30$ μm) match the physical properties of the device. As a simple first-order equivalent circuit can model the parasitics well, this investigation also justifies the single parasitic pole as modeled in Eq. (1). Furthermore, we measured the relative intensity noise (RIN) spectrum and could clearly observe the relaxation pole as a peak. This investigation was also in agreement with pole extraction from curve-fitting.

The transmission performance of our VCSELs was evaluated to highlight their feasibility as directly modulated transmitters in broadband optical communication systems. Error-free transmission over 20 km of the most widely deployed standard single-mode fiber (SSMF) with monolithically integrated one-dimensional arrays has been demonstrated recently at the wavelength of 1550 nm[20]. The transmission performance of the VCSEL array was evaluated under direct modulation at 10 Gb/s with non-return-to-zero (NRZ) data of $2^{15} - 1$ pseudo random bit pattern length. The transmission experiment was carried out over an amplifier-free 20-km SSMF link. A 12.5-GHz photodiode with a 10-GHz limiting amplifier, followed by a 9.33-GHz low-pass filter was used. Figure 6 shows the superimposed optical spectrum from four 10-Gb/s modulated channels spaced at 100 GHz on the ITU-grid.

The layout of these devices is presented as inset in Fig. 6. Further, bit-error-rate (BER) measurements of all channels are shown in Fig. 7, providing error free operation under all biasing conditions. Note that there was no BER penalty in among all channels with widely spreading bias from 3.3 to 7.6 mA. Corresponding eye-diagrams at a BER of 10^{-9} are shown as inset. The timing jitter in eye diagrams as well as the low sensitivity may be attributed to the use of a preliminary laser-mounting on sub-miniature (SMA) mount. At a modulation rate of 10 Gb/s, the line broadening due to adiabatic chirp

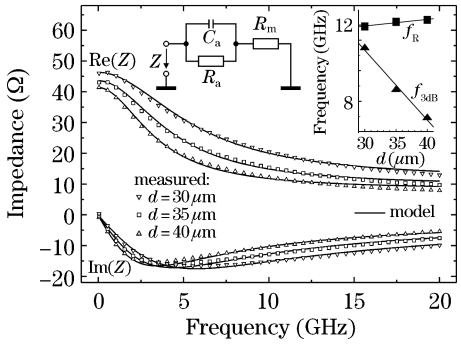

Fig. 5. Real and imaginary part of chip impedance Z against frequency for different chip diameters d. Equivalent circuit and dependence of resonance frequency $f_{\rm R}$ and modulation bandwidth $f_{\rm 3dB}$ on chip diameter d are shown in insets.

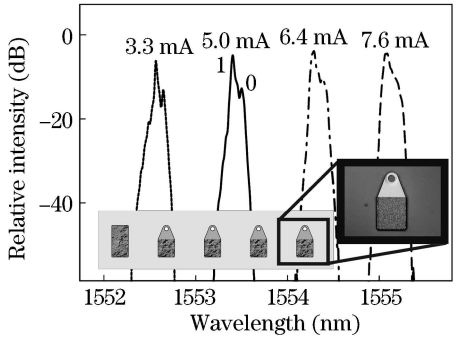

Fig. 6. Spectrum of a 1 × 4 array of electro-thermally tuned 1.55-μm VCSELs under modulation at 10 Gb/s. WDM (100-GHz spacing) channels are addressed by current tuning. Layout and top view of VCSEL array are given as inset.

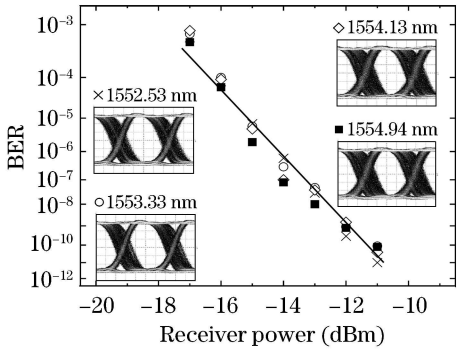

Fig. 7. BER performance of 10-Gb/s modulated VCSEL array over 20-km SSMF. WDM channels are addressed without BER penalty. Corresponding eye diagrams are given as insets.

was measured to be less than the 100-GHz or 50-GHz channel spacing, respectively. Different from arrays of classical edge emitters, VCSEL arrays can be used in an upgrade of CWDM to dense wavelength division multiplexing (DWDM) networks due to their flat bandwidth behavior and large tuning ability. Even for DWDM grids of 50 GHz, there is no crosstalk due to adiabatic chirp. For 100/50 GHz DWDM grids, at least 4/8 channels at 10 Gb/s can be addressed only by varying the laser biasing condition. Our transmission results highlight the potential of the VCSELs as uncooled transmitters in CWDM access networks. Additionally, these VCSELs can also work under injection-locking with enhanced modulation bandwidth and stabilized wavelength or managed chirp and can therefore be readily applied as upstream transmitters in passive optical networks[21,22]. By adjusting the biasing conditions for maximum reach, using the self-steepening effect, i.e., dispersion compensation by self-phase modulation due to laser chirp, a power-limited reach on SSMF of 65 km at a BER of 10^{-3} and 10.7 Gb/s could be demonstrated[23]. Passive dispersion compensation fibers can be used to achieve better performance[24]. Moreover, optically injection-locked VCSELs can also be utilized as duplex transmitters/receivers redundantizing separate photodetectors[25].

For classical DWDM solutions, one dedicated laser per channel is used. For failsafe operation, one spare laser per channel would be needed, causing high system cost. Therefore, widely (i.e., tens nanometers at 1.3 and 1.55 μm) tunable laser sources are highly demanded for fiber-based communication. Fig. 8 schematically shows the tuning behavior of a widely micro-electro-mechanical system (MEMS) tunable VCSEL as presented in Fig. 2. A typical spectrum and an envelope function, generated by keeping track of the maximum of the laser spectrum during tuning with constant pump current is shown. The tuning range as defined by SMSR > 30 dB typically exceeds 50 nm at 1.55 μm with a very high spectral purity and nearly constant output power. Due to the external cavity, widely tunable VCSELs with apertures exceeding 10 μm are still highly single mode and fiber-coupled powers of several milliwatts have been achieved[26].

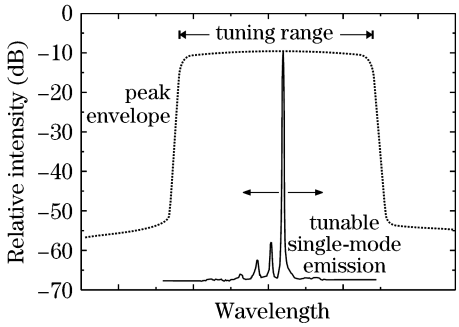

Fig. 8. Schematic characteristics of a MEMS-tunable VCSEL. For MEMS-tunable BTJ-VCSELs at 1.55 μm, a tuning range over 50 nm has already been demonstrated[17].

With their inherent electro-thermal tunability of several nanometers, low cost potential, low power consumption, and spectral purity, VCSELs are ideal light sources for TDLS. In VCSEL spectrometers, the tunable single-mode emission line of the laser with a linewidth much smaller than the absorption-line ($\sim$ 10 MHz versus $\sim$ 1 GHz) can be used to scan a selected resonance absorption peak of the gas under investigation. Therefore, the VCSEL wavelength must match the resonance frequency of the molecule of interest[13]. Especially, the wavelength regime from 1 to 3 μm is of great interest, as many relevant gases have characteristic absorption lines in that range and photo detectors provide sufficient signal-to-noise ratio without cooling necessity. Up to now, the BTJ technology can provide InP-based long-wavelength VCSELs from 1.3 to 2.3 μm and our current research focus is on GaSb-based VCSELs, targeting wavelengths from 2.3 to 3 μm[16].

For tailoring the emission wavelength of a long-wavelength VCSEL, active region, laser cavity, and mirrors have to be matched. Figure 9(a) illustrates this principle presenting photoluminescence (PL) at room temperature together with the Bragg mirror reflectivity. The final laser emission for various bias currents is depicted in Fig. 9(b). An emission wavelength of 2360 nm has been achieved which can be tuned over 6 nm by varying the driving current from 4 to 10 mA. The SMSR is setup-resolution-limited and always above 25 dB. With this device, carbon monoxide was detected using TDLS with high sensitivity[15].

The absorption lines of many gases can be found in the high-resolution transmission molecular absorption database (HITRAN)[27]. Figure 10 shows the "fingerprint" of H_2O in the light output versus current (L-I) curve and the tuning characteristic of a 1.8-μm VCSEL as inset. In order to demonstrate the applicability of the BTJ-VCSEL in TDLS, we built an easy tabletop

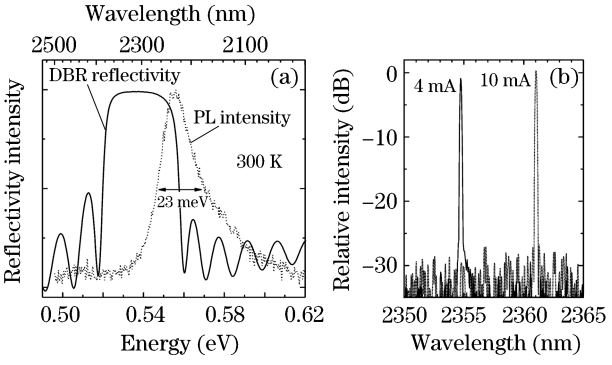

Fig. 9. (a) Reflectivity (solid line) and PL intensity (dotted line) of a 2.3-μm InP-based long-wavelength VCSEL structure and (b) current dependent output spectra.

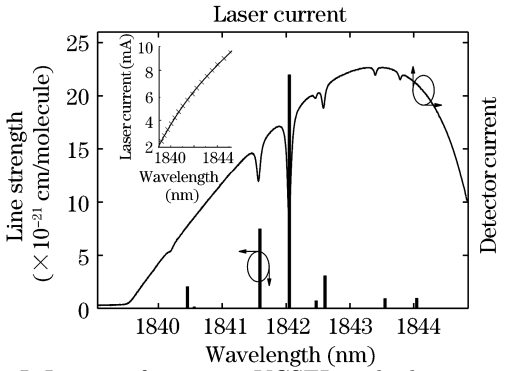

Fig. 10. *L-I*-curve of a 1.8-μm VCSEL with absorption peaks of water according to the HITRAN database. VCSEL tuning characteristic is presented as inset.

unit as demonstrator, which measures the humidity of air with high precision. The VCSEL is directly driven by an easy microcontroller which also evaluates the photo detector. We do not use any temperature control, but software which automatically chooses the best absorption line in range for evaluation. As water shows rather strong absorption peaks, we directly evaluate the absolute absorption[13].

Single-mode and tunable VCSELs in the near to mid-infrared are available with superior lasing characteristics. The monolithic BTJ concept on InP covers the entire wavelength range from 1.3 to 2.3 μm with enormous application potential from telecommunications to sensing. Mid-infrared VCSELs based on GaSb have also been published. In the wavelength range from 1.3 to 1.6 μm, high-speed VCSELs feature high modulation bandwidth above 10 GHz and low power consumption. Moreover, VCSEL arrays can be monolithically fabricated, enabling multi-channel and wavelength division multiplexing (WDM) applications. In a two-chip design with a MEMS mirror, a tuning range of more than 50 nm is possible. Furthermore, with emission wavelengths up to 2.3 μm, inherent continuous tunability, and typical SMSR of the order of 40 dB, these lasers are ideal light sources for TDLS. In summary, BTJ long-wavelength VCSELs are highly innovative key components for a variety of future growth markets from the telecommunications to instrumentation, measurement, and process control.

This work was partly funded by the German Research Council (DFG), the National Natural Science Foundation of China (No. 60510173 and 60506006), the European Union via NEMIS (No. FP6-2005-IST-5-031845), and the German Federal Ministry of Education and Research via NOSE (No. 13N8772). M.-C. Amann's e-mail address is amann@wsi.tum.de.

References

1. K. Iga, IEEE J. Sel. Top. Quantum Electron. **6,** 1201 (2000).
2. F. Koyama, J. Lightwave Technol. **24,** 4502 (2006).
3. R. Shau, M. Ortsiefer, J. Rosskopf, G. Böhm, C. Lauer, M. Maute, and M.-C. Amann, Proc. SPIE **5364,** 1 (2004).
4. M. Ortsiefer, M. Grau, J. Rosskopf, R. Shau, K. Windhorn, E. Rönneberg, G. Böhm, W. Hofmann, O. Dier, and M.-C. Amann, *IEEE 20 th International Semiconductor Laser Conference* 113 (2006).
5. M. Ortsiefer, S. Baydar, K. Windhorn, G. Böhm, J. Rosskopf, R. Shau, E. Rönneberg, W. Hofmann, and M.-C. Amann, IEEE Photon. Technol. Lett. **17,** 1596 (2005).
6. J. Boucart, G. Suruceanu, P. Royo, V. I. Iakovlev, A. Syrbu, A. Caliman, A. Mereuta, A. Mircea, C.-A. Berseth, A. Rudra, and E. Kapon, IEEE Photon. Technol. Lett. **18,** 571 (2006).
7. C.-K. Lin, D. P. Bour, J. Zhu, W. H. Perez, M. H. Leary, A. Tandon, S. W. Corzine, and M. R. T. Tan, IEEE J. Sel. Top. Quantum Electron. **9,** 1415 (2003).
8. A. Ramakrishnan, G. Steinle, D. Supper, C. Degen, and G. Ebbinghaus, Electron. Lett. **38,** 322 (2002).
9. W. Hofmann, N. H. Zhu, M. Ortsiefer, G. Böhm, Y. Liu, and M.-C. Amann, Electron. Lett. **42,** 976 (2006).
10. M. Yamada, T. Anan, H. Hatakeyama, K. Tokutome, N. Suzuki, T. Nakamura, and K. Nishi, IEEE Photon. Technol. Lett. **17,** 950 (2005).
11. N. Nishiyama, C. Caneau, B. Hall, G. Guryanov, M. H. Hu, X. S. Liu, M.-J. Li, R. Bhat, and C. E. Zah, IEEE J. Sel. Top. Quantum Electron. **11,** 990 (2005).
12. V. Iakovlev, G. Suruceanu, A. Caliman, A. Mereuta, A. Mircea, C.-A. Berseth, A. Syrbu, A. Rudra, and E. Kapon, IEEE Photon. Technol. Lett. **17,** 947 (2005).
13. C. Lauer, S. Szalay, G. Böhm, F. Köhler, and M.-C. Amann, IEEE Trans. Inst. Meas. **54,** 1214 (2005).
14. G. Böhm, M. Grau, O. Dier, K. Windhorn, E. Rönneberg, J. Rosskopf, R. Shau, R. Meyer, M. Ortsiefer, and M.-C. Amann, J. Crys. Growth **301-302,** 941 (2007).
15. A. Hangauer, J. Chen, R. Strzoda, M. Ortsiefer, and M.-C. Amann, Opt. Lett. **33,** 1566 (2008).
16. A. Bachmann, T. Lim, K. Kashani-Shirazi, O. Dier, C. Lauer, and M.-C. Amann, Electron. Lett. **44,** 202 (2008).
17. M. Maute, B. Kögel, G. Böhm, P. Meissner, and M.-C. Amann, IEEE Photon. Technol. Lett. **18,** 688 (2006).
18. H. P. Huang, N. H. Zhu, and J. Liu, IEEE Photon. Technol. Lett. **17,** 2155 (2005).
19. L. Chrostowski, B. Faraji, W. Hofmann, M.-C. Amann, S. Wieczorek, and W. W. Chow, J. Sel. Top. Quantum Electron. **13,** 1200 (2007).
20. W. Hofmann, E. Wong, G. Böhm, M. Ortsiefer, N. H. Zhu, and M. C. Amann, IEEE Photon. Technol. Lett. **20,** 291 (2008).
21. E. Wong, X. Zhao, C. J. Chang-Hasnain, W. Hofmann, and M.-C. Amann, IEEE Photon. Technol. Lett. **18,** 2371 (2006).
22. X. Zhao, Y. Zhou, C. J. Chang-Hasnain, W. Hofmann, and M.-C. Amann, Opt. Express **14,** 10500 (2006).
23. F. Fidler, C. Hambeck, P. J. Winzer, and W. R. Leeb, in *Proceedings of European Conference on Optical Communication (ECOC)* **3,** 521 (2006).
24. L. Grüner-Nielsen, M. Wandel, P. Kristensen, C. Jørgensen, L. V. Jørgensen, B. Edvold, B. Pálsdóttir, and D. Jakobsen, J. Lightwave Technol. **23,** 3566 (2005).
25. Q. Gu, W. Hofmann, M.-C. Amann, and L. Chrostowski, IEEE Photon. Technol. Lett. **20,** 463 (2008).
26. M. Maute, G. Böhm, M.-C. Amann, B. Kögel, H. Halbritter, and P. Meissner, Opt. Express **13,** 8008 (2005).
27. L. S. Rothman, A. Barbe, D. C. Benner, L. R. Brown, C. Camy-Peyret, M. R. Carleer, K. Chance, C. Clerbaux, V. Dana, V. M. Devi, A. Fayt, J.-M. Flaud, R. R. Gamache, A. Goldman, D. Jacquemart, K. W. Jucks, W. J. Lafferty, J.-Y. Mandin, S. T. Massie, V. Nemtchinov, D. A. Newnham, A. Perrin, C. P. Rinsland, J. Schroeder, K. M. Smith, M. A. H. Smith, K. Tang, R. A. Toth, J. Vander Auwera, P. Varanasi, and K. Yoshino, J. Quantum Spectrosc. Radiat. Transfer **82,** 5 (2003).